ACS APPLIED ENERGY MATERIALS

www.acsaem.org Article

Enhancement of Electrocatalytic CO_2 Reduction to Methane by CoTMPyP when Hosted in a 3D Covalent Graphene Framework

Yair Bochlin, Lior Ezuz, Yanir Kadosh, Daniel Benjamin, Yuval Mordekovitz, Shmuel Hayun, Eli Korin, and Armand Bettelheim*

Cite This: *ACS Appl. Energy Mater.* 2021, 4, 10033−10041 Read Online

ACCESS | Metrics & More | Article Recommendations | Supporting Information

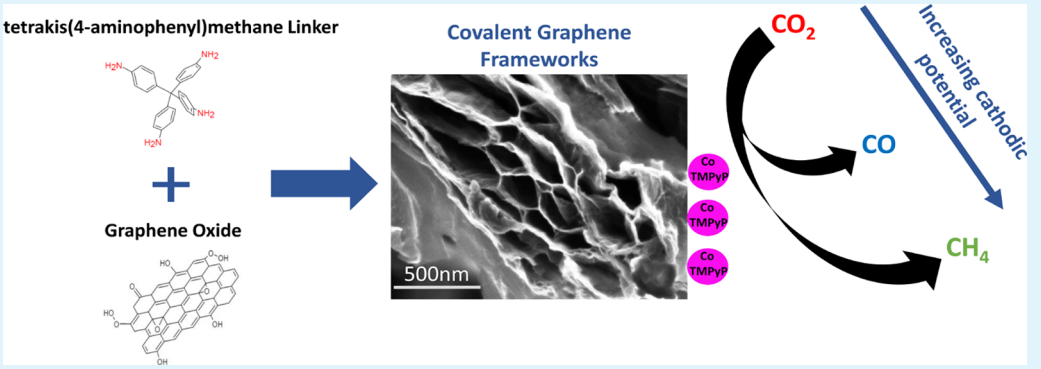

ABSTRACT: Electrocatalytic reduction of carbon dioxide is a promising technique to convert CO_2 into useful products and to aid environmental concerns. Here, we report on the preparation of a unique three-dimensional graphene-based structure, covalent graphene framework (CGF), which is obtained by the chemical attachment of a nitro-functionalized graphene derivative to a 3D aniline-based linker. CGF is then used to host cobalt [5,10,15,20-(tetra-*N*-methyl-4-pyridyl)porphyrin] (CoTMPyP) as a catalyst for electrochemical CO_2 reduction. The porous structure of CGF with free amine functional groups enables strong irreversible adsorption of CO_2 which promotes the formation and stabilization of a key carbamate intermediate. The combined CGF−CoTMPyP catalytic system shows enhanced performance for the $8e^-$ CO_2 reduction to CH_4 (faradaic efficiency ~20%) at −0.72 V versus RHE in aqueous solutions. This work emphasizes the importance of tuning the morphology and chemical composition of the catalyst surroundings in the design of efficient catalytic systems in the field of energy conversion.

KEYWORDS: *CO_2 reduction, covalent graphene frameworks, cobalt porphyrin, electrocatalysis, methane, CO, carbamate, azo-bridges*

INTRODUCTION

The constantly increasing concentration of atmospheric carbon dioxide is considered to be the most significant environmental issue facing mankind today, and in order to meet the international global warming of less than 2 °C, CO_2 emissions must be drastically reduced.[1,2] Since transportation and industrial processes are major contributors to CO_2 emissions, developing innovative energy generation processes is key in reaching the desired goal.[3−5] Much effort is devoted to developing efficient processes for the separation, capture, and storage of CO_2 that will enable its utilization as a feedstock for its conversion into useful materials.[6,7] CO_2 conversion by electrochemistry powered by energy from renewable resources is a promising technology that can utilize CO_2 and reduce it to useful fuels and chemicals.[8−10] Still, an efficient electrocatalyst is required since thermodynamic and kinetic barriers are associated with the reorganizational energy required to bend the stable CO_2 molecule to the $CO_2^{\bullet-}$ radical anion (−1.9 V vs normal hydrogen electrode[11]).

Metalloporphyrins and similar compounds are widely researched as catalysts for the CO_2 reduction reaction (CO_2RR) due to their well-defined structure and ability to be precisely modified for specific applications. A recent study reported on the various possible degradation mechanisms of cobalt porphyrin-based electrocatalysts which allow to gain an in-depth knowledge of the long-term stability of the electrocatalytic processes.[12] Among all transition-metal centers, cobalt and iron ions have been found to be the most active for CO_2RR.[13,14] Covalent and noncovalent functionalizations of metalloporphyrins with various carbon materials are commonly used for immobilization purposes and to enhance their

Received: July 6, 2021
Accepted: August 19, 2021
Published: September 1, 2021

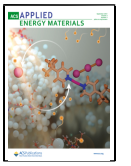

catalytic performance.[15] Carbon materials, such as graphene[16] and carbon nanotubes,[17] are regularly used because of their good conductivity, durability, and aromatic nature with delocalized π electrons that facilitate rapid electron transfer from the electrode. In this respect, 3D graphene structures obtained by a variety of preparation procedures[18−20] have been considered for rapid adsorption of CO_2 from flue gas.[21,22] However, although carbon supports proved to be efficient in increasing the catalytic activity of metalloporphyrins, they have failed to push the reaction beyond two electron products with cobalt porphyrins: CO is generated selectively in most cases with some reports demonstrating formate production.[17,23,24] One exception is CO_2 reduction to CH_4 using cobalt protoporphyrin IX in acidic conditions at −1.38 V vs standard hydrogen electrode, although with a faradaic efficiency (FE) of only <1%.[25] Iron porphyrins were also found to be especially selective toward the production of CO from electrochemical CO_2 reduction.[16,26] However, under unique photochemical conditions, iron porphyrin has been reported to also produce CH_4.[27] Cu-based complexes such as polycrystalline copper with pyridinum additives,[28] Cu-phthalocyanines,[29,30] and Cu-porphyrins[31] are regularly reported as highly active for CO_2RR to CH_4 and C_{2+} products with FEs that reach up to 66%. However, these electrocatalysts require high overpotentials [<−1 V vs reversible hydrogen electrode (RHE)] for the activation of the catalyst which results in a high energy amount that is required for the process.

We have reported on a combined experimental and density functional theory investigation of CO_2 electrocatalytic reduction by dissolved cobalt [5,10,15,20-(tetra-*N*-methyl-4-pyridyl)porphyrin] (CoTMPyP) in neutral aqueous solutions[32] and further explored this catalyst when immobilized in electrochemically produced coatings of reduced graphene oxide (rGO).[33] Inspired by the relatively easy preparation procedures, diverse applications, and stability of covalent organic frameworks (COFs),[34,35] we synthesized a graphene structure obtained by covalent attachment of a nitro-graphene derivative to an organic linker playing two important roles: imparts a 3D graphene configuration and chemically adsorbs CO_2 due to the presence of its aniline sites. We show in the present report that such a new covalent graphene framework (CGF) can be used to host catalysts, such as CoTMPyP, and the combined system shows unique features regarding the products of CO_2 electrocatalytic reduction: formation at certain conditions of a relatively high faradaic yield (~20%) of the unexpected methane $8e^-$ reduction product at a moderate applied potential (maximum activity at −0.72 V vs RHE).

EXPERIMENTAL SECTION

Materials. Single-layer GO was purchased from ACS material. Nitric acid (70%), sulfuric acid (95−98%), potassium hydroxide (KOH), *N*,*N*-dimethylformamide (DMF) (99.8%), tetrahydrofuran (THF) anhydrous (≥99.9%), acetone (99.9%), and tetrakis(4-aminophenyl)methane (TAPM) (≥90%) were purchased from Sigma-Aldrich. CoTMPyP tetrachloride was obtained from Porphy-Chem.

Synthesis Procedures. *Synthesis of Nitrated Graphene Oxide.* 50 mL of concentrated sulfuric acid solution was slowly added into 25 mL of concentrated nitric acid. This acid mixture was cooled to room temperature using an ice bath. At the same time, 100 mg of GO and 25 mL of concentrated sulfuric acid solution were added into a beaker and sonicated for 30 min. Then, the acid mixture was slowly dropped into the beaker, while the reaction system was stirred for 5 h at 45 °C. Thereafter, the mixture was diluted and cooled with deionized (DI) water in order to terminate the reaction. Finally, the resulting precipitate was centrifuged, washed with deionized water until pH of 7 was attained, and dried at 60 °C for 5 h under vacuum.

Synthesis of CGF. The obtained nitro-doped graphene oxide (NGO) (0.30 g), TAPM (0.60 g, 1.58 mmol), and KOH (1.62 g, 28.87 mmol) were dissolved together in DMF (60 mL). The reaction mixture was heated to 150 °C and stirred for 24 h under an argon atmosphere. The reaction mixture was cooled to room temperature and added to 100 mL of distilled water. The black sediment was centrifuged and washed three times with distilled water, acetone, and THF in order to remove any unreacted materials and KOH. Subsequently, the resulting material was dried at 500 °C under vacuum for 12 h.

Characterization Methods. Fourier transform infrared spectroscopy (FTIR) was performed by a VERTEX 80v vacuum spectrometer at a scan range of 500−4000 cm^{-1}. The sample powders were ground with KBr and pressed into pellets. X-Ray photoelectron spectroscopy (XPS) was performed using a Thermo Fisher scientific ESCALAB 250 with an Al Kα X-ray source and a monochromator. Scanning electron microscopy (SEM) was performed using a FEI Quanta 200 scanning electron microscope. Transmission electron microscopy (TEM) images were obtained using a JEOL JEM 2100F transmission electron microscope coupled with an energy-dispersive X-ray spectroscopy (EDS) detector.

Gas Adsorption Analysis. Adsorption/desorption isotherms were collected using a Micromeritics ASAP 2020 (Micromeritics, Norcross, GA) instrument. A full N_2 adsorption/desorption isotherm was collected at −196 °C. From this isotherm, 10 points in the P/P^0 relative pressure range (P^0 = saturation pressure) of 0.05−0.30 were used to determine the amount of surface area utilizing the Brunauer−Emmett−Teller model. Prior to analysis, each sample was degassed under vacuum at 400 °C for 4 h. CO_2 adsorption/desorption isotherms were collected at 25 °C to a maximal pressure of 800 mmHg.

Electrode Preparation. CGF powder was initially dispersed in an aqueous solution containing 0.1% Nafion and sonicated for 3 h. Then, CoTMPyP was added to the dispersion which initiated the spontaneous aggregation and precipitation of the materials in the bottom of the vial. After formation of the agglomerates, they were separated from the solution by centrifugation and redispersed in DI water by vigorous mixing with a vortex mixer. 100 μL of the final dispersion was drop-casted onto each side of a carbon paper electrode, which was then dried overnight at ambient conditions in a fume hood.

Electrochemical Measurements. The electrochemical analysis was conducted using a PINE WaveDriver 20 bipotentiostat/galvanostat with AfterMath software. A homemade three-electrode electrochemical cell was used with the drop-coated carbon paper as the working electrode, platinum wire counter electrode (99.9%, Sigma-Aldrich) separated by a fritted glass tube (PINE research), and an Ag/AgCl (sat. KCl) reference electrode (CH Instruments). 0.1 M $NaHCO_3$ was used as the electrolyte for the electrochemical measurements (pH 8.3 and 6.8 in the absence and presence of CO_2, respectively). Due to the known electroactivity of cobalt porphyrins toward O_2 reduction, thorough deaeration of the solutions with Ar was carried out before performing measurements of CO_2 reduction. Cyclic voltammograms were recorded after the solution was saturated with Ar or CO_2 by purging the gas through the solution for at least 15 min. Steady-state chronoamperometry measurements were performed with a continuous flow of CO_2 through the electrolyte.

The reported potentials were converted from the Ag/AgCl scale to the RHE scale using the following formula

$$E(\text{vs RHE}) = E(\text{vs Ag/AgCl}) + 0.2V + 0.059 \times \text{pH}$$

Product Analysis. Controlled potential electrolysis experiments were carried out in an airtight electrochemical cell (BioLogic). The measurement data were recorded using a BioLogic SP-50 potentiostat/galvanostat with EC-Lab software. The CGF−CoTMPyP-coated

https://doi.org/10.1021/acsaem.1c01978
ACS Appl. Energy Mater. 2021, 4, 10033−10041

Scheme 1. Synthesis of CGF from GO by Direct Coupling of Aromatic Nitro and Amino Groups

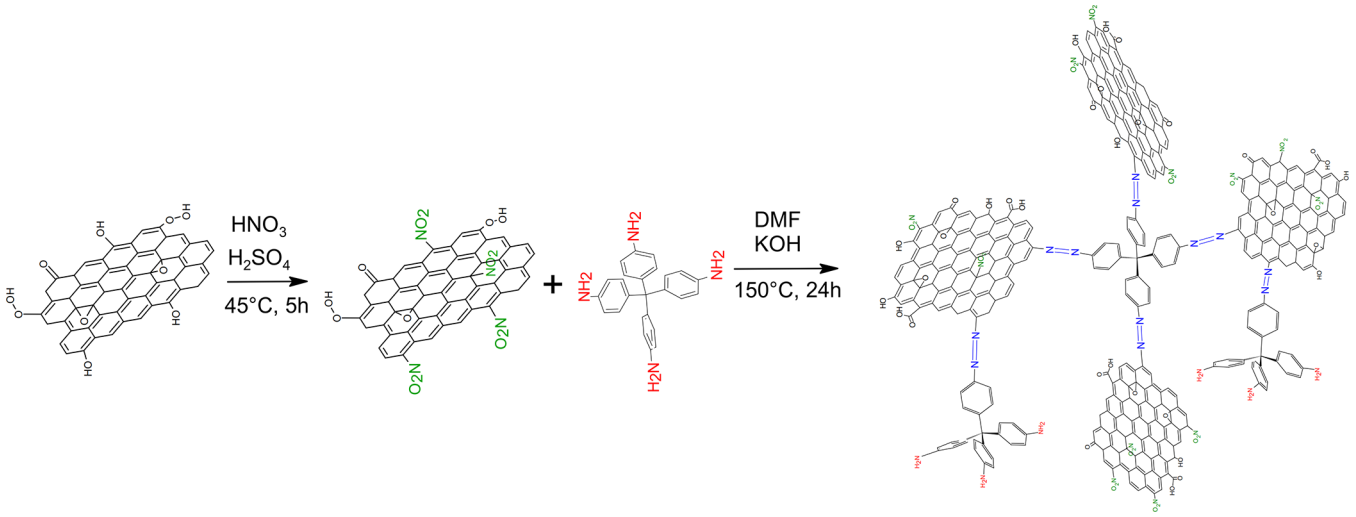

carbon paper electrode was used as the working electrode (geometrical surface area of 1 cm^2), Ag/AgCl (Metrohm) was used as the reference electrode, and Pt wire in a glass fritted tube was used as the counter electrode. During electrolysis, a constant flow of CO_2 (5 mL min^{-1}) was maintained using a mass flow controller (MKS P4B.) The product gas stream was continuously analyzed with a gas chromatograph (GC). Ar was used as the carrier gas for improved detection of hydrogen. The GC (SRI 8610C in a Multi Gas #5 configuration) was equipped with 0.5 and 2 m Hayesep D columns, 2 m Molecular sieve 5 A column, a thermal conductivity detector (TCD), and a flame ionization detector (FID) which was fitted with a methanizer. CO and unreacted CO_2 were detected with the FID detector (after conversion to methane in the methanizer), and hydrogen was detected with the TCD. The product gas stream was sampled every 20 min in order to quantify the products. The fraction of the products was determined by calibration using a gas mixture with known concentration (SCOTTY). The FE was calculated using the following formula

$$FE(\%) = \frac{z_i \times F \times x_i \times F_m}{I} \times 100$$

where z_i is the number of electrons needed for the reaction to a specific product (2 for CO and 8 for CH_4), F is Faraday's constant, x_i is the fraction of the product in the gas stream (determined from the GC), F_m is the molar flow rate of CO_2, and I is the total current.

RESULTS AND DISCUSSION

Azo-linked polymers[36] and COFs[37−39] can be obtained by direct coupling of aromatic amino and nitro groups. The new CGF was synthesized by first converting GO powder into NGO by a previously described process.[40] NGO was then reacted with the 3D TAPM linker according to reported azo-linked polymers and COF preparation procedures (see details in the Supporting Information). The resulting material possesses a unique three-dimensional structure with available amine functional groups (Scheme 1), and it is used as a support for a CO_2 reduction catalyst.

The chemical structure and functional groups of the CGF was confirmed by FTIR and XPS (Figure 1A,B, respectively). The FTIR spectrum of GO presents several characteristic bands that correspond to oxygen functional groups, such as those appearing at 3400 (O−H stretching), 1720 (C═O), 1620 (aromatic C═C), and 1060 cm^{-1} (C−O).[41] After the conversion of GO to NGO, a new band appears at 1240 cm^{-1} which is attributed to a newly formed C−N bond.[42−44] In addition, a band observed at 1390 cm^{-1} is attributed to the symmetric stretching of NO_2 groups.[45] The characteristic asymmetric stretching of NO_2 groups at 1600−1650 cm^{-1} could not be observed due to overlapping with the aromatic C═C bond.[40] After the formation of CGF, a band appears at 1510 cm^{-1} which is ascribed to the N═N azo bond.[46] Additional signals at 820 cm^{-1} (for out of plane N−H vibration[47]) and 1390 cm^{-1} (asymmetric NO_2 stretching) suggest the presence of unreacted amino and nitro groups. The high-resolution C 1S XPS spectrum of CGF (Figure S1) can be deconvoluted to four peaks at 284.8, 285.6, 288.2, and 289.2 eV that correspond to C═C/C−C (45.7 at %), C−OH/C−N (31.6 at %), C═O (9.6 at %), and O−C═O (13.1 at %) bonds.[40,47−49] Notably, the relative amount of C−OH bonds, which overlap with C−N moieties, is significantly higher as compared to GO in which C−O−C groups prevail[33] and could not be detected in CGF. Furthermore, the high content of carboxylic groups observed for CGF is most likely due to the strong oxidizing conditions used in the synthesis process. The N 1S spectrum (Figure 1B) reveals two contributions at 400.3 and 399.2 eV. The former is attributed to the newly formed azo groups,[50] while the latter is assigned to either unreacted amino groups[40] or remaining nitro groups that are probably reduced by X-ray irradiation during the analysis.[51] The total atomic content of nitrogen in the sample is 1.3%, out of which 0.57% are azo bonds.

The morphology of the CGF powder was examined using high-resolution SEM. The images in Figure 1C show a three-dimensional porous structure that is very different from the characteristic wrinkled structure of GO.[52−54] It is likely that the azo bridges are formed both in plane and on the edges of the graphene sheets. This seems to lead to the formation of irregular structures containing pores with sizes in the ∼0.2−1 μm range, including honeycomb-like ones as depicted in the inset of Figure 1C.

The N_2 adsorption/desorption isotherm at 77 K (Figure S2) resembles a type II isotherm, representing unrestricted monolayer−multilayer adsorption which is typical of macroporous materials.[55] This observation is consistent with the SEM images that show pore sizes in the micrometer scale. A CO_2 adsorption/desorption isotherm at 298 K is presented in Figure 1D and shows more massive CO_2 adsorption than desorption. This indicates that CO_2 is strongly and irreversibly adsorbed onto the CGF surface. Strong interactions with

https://doi.org/10.1021/acsaem.1c01978
ACS Appl. Energy Mater. 2021, 4, 10033−10041

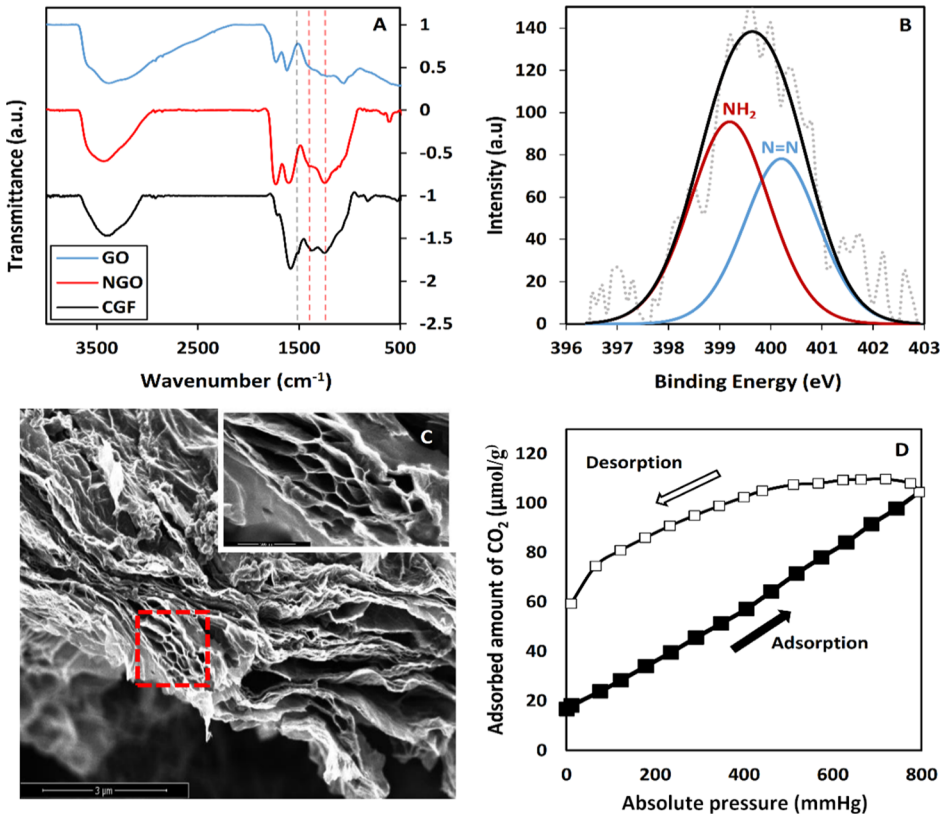

Figure 1. Characterization of the obtained CGF powder. (A) Transmission FTIR spectra of GO, NGO, and CGF samples. Vertical lines show the position of the characteristic peaks for each sample. (B) XPS N 1S spectrum of CGF. (C) SEM image of CGF (inset: enlargement of the marked area). (D) CO_2 adsorption (filled symbols) and desorption (open symbols) isotherms at 298 K of the CGF powder.

various nitrogen groups are likely to cause this phenomenon which was previously observed in amine-based membranes for CO_2 transport.[56,57] These interactions between amine groups and CO_2 have been suggested to involve the formation of carbamate species which have been exploited both for combined carbon capture and recycling of CO_2 to fuels.[34,58−60] The formation of carbamate species was confirmed by FTIR spectroscopy of CGF before and after exposure to CO_2 (Figure S3). Two new peaks appear at 1629 and 1649 cm^{-1} in the spectrum of the exposed CGF, representing a newly bound carbamate species.[34] Azo groups present in CGF could also play a role in the steep rise at low pressure observed in the CO_2 isotherms, such as it has been associated with high binding energies of CO_2 to azo groups present in azo-porous organic frameworks.[61] This has been ascribed to a strong dipole−quadrupole interaction between the polarizable CO_2 molecules and the nitrogen sites on the azo group.[62] The amount of adsorbed CO_2 increases with the increase of CO_2 pressure and reaches a maximum of 110 μmol g^{-1} at 800 mmHg. This value is comparable to some organic CO_2 capturing materials such as organic amide polymers,[63] covalent triazine frameworks,[64] and graphitic nanoribbons.[65] The irreversible adsorbed amount of CO_2 is 59 μmol g^{-1} which corresponds to an occupied surface of 5 m^2 g^{-1}, using the CO_2 molecular area of 0.142 nm^2.[65] This occupied surface area by irreversibly adsorbed CO_2 molecules is ∼55% of the total surface area (9.1 m^2 g^{-1}).

To prepare CoTMPyP−CGF composites (CoP−CGF), CGF was first dispersed in an aqueous solution using sonication with the addition of 0.1% of Nafion solution. The resulting black ink was mixed with an aqueous solution containing various amounts of dissolved CoTMPyP. Upon mixing, the composites spontaneously aggregated and precipitated in the bottom of the vial (Figure S4). CGF and CoTMPyP presumably interact through electrostatic interactions between the positively charged porphyrin and the negatively charged CGF followed by $\pi-\pi$ interactions as also reported for other porphyrin−graphene systems.[26,33,66] Increasing the CGF/CoTMPyP wt/% ratio caused the supernatant solution to gradually become colorless (Figure S4), as also indicated by the disappearance of the typical CoTMPyP spectrum (Figure S5) at a wt/% ratio of 3.5. High-angle annular dark-field scanning transmission electron microscopy (HAADF-STEM) and EDS mapping were used to characterize CoP−CGF. The STEM image (Figure 2A) shows that the composite forms large micron-sized agglomerates, and according to EDS, C, N, and Co elements are homogeneously distributed throughout the composite structure (Figure 2B−D, respectively). The EDS spectrum (Figure S6) shows distinct signals for all these elements with a cobalt catalytic site content of 0.98 At %.

In order to examine the electrocatalytic activity for CO_2 reduction, the CoTMPyP−CGF precipitate was separated from the solution, redispersed in water by sonication, and drop-coated on carbon paper serving as the working electrode. The electrochemical behavior of the CoTMPyP−CGF coatings was first examined by cyclic voltammetry (Figure 3A) in N_2- and CO_2-saturated 0.1 M $NaHCO_3$ aqueous solution (pH values 8.3 and 6.8, respectively). Under both CO_2 and N_2 atmospheres, three reduction waves with onset potentials of 0.4, 0, and −0.2 V versus the RHE were observed. The first two waves are ascribed to the reduction of oxygen functional

https://doi.org/10.1021/acsaem.1c01978
ACS Appl. Energy Mater. 2021, 4, 10033−10041

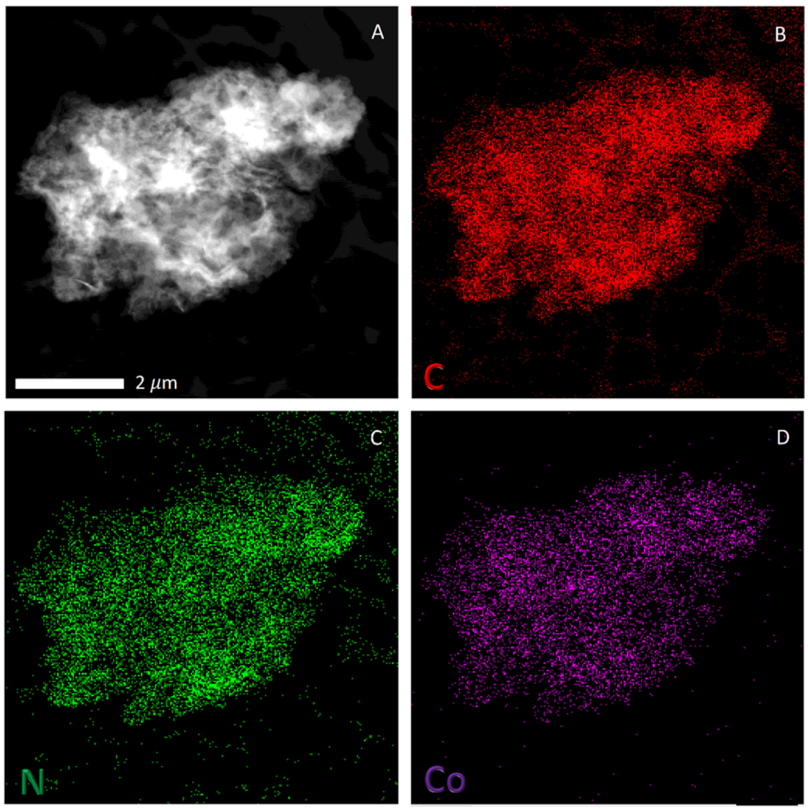

Figure 2. HAADF-STEM image of CoP−CGF (A) and the corresponding EDS maps of C, N, and Co (B, C, and D, respectively).

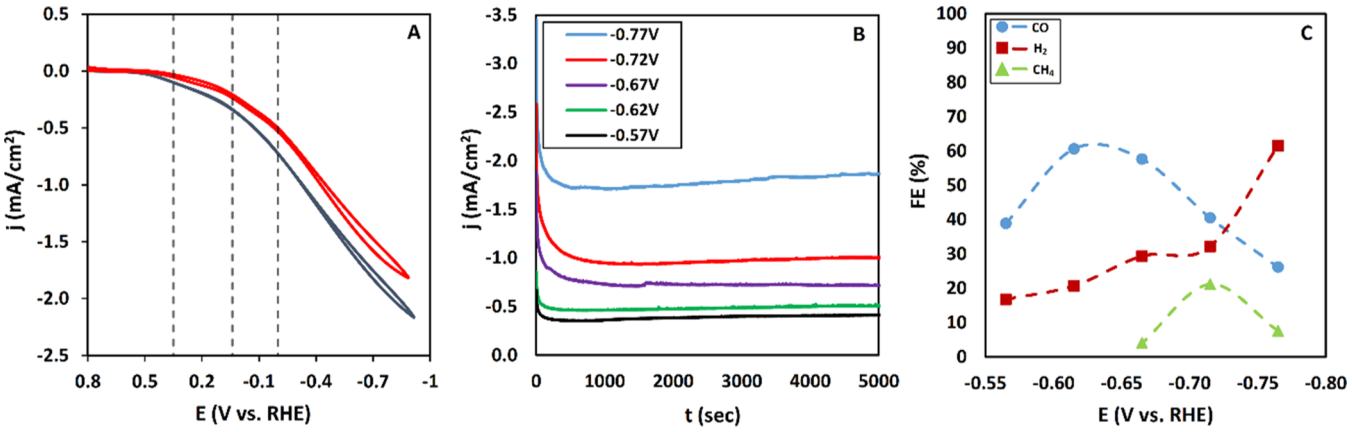

Figure 3. (A) Cyclic voltammograms of CoPCGF coated on carbon paper electrodes in N_2- (blue) and CO_2 (red)-saturated 0.1 M $NaHCO_3$ at 25 mV/s. Vertical lines show the onset potentials of waves. (B) Chronoamperometry curves for CoPCGF coatings under a continuous flow of CO_2 (10 cc/min) in 0.1 M $NaHCO_3$ at different applied potentials. (C) Corresponding FEs obtained for CoPCGF coatings at each applied potential.

groups that originate from GO.[53] The wave appearing at the most cathodic potential is assigned to the combined CO_2RR and hydrogen evolution reaction processes. It is observed that the current densities under a N_2 atmosphere are higher as compared to those under CO_2 atmosphere, reaching 2.2 and 1.8 mA cm^{-2}, respectively, at a potential of −0.9 V. This phenomenon was previously observed and described as reduction of CO_2 on active catalytic sites with slower kinetics and mass transport than that of the competing HER, consequently inhibiting this reaction.[26,67]

To test the stability of the CoP−CGF-coated electrode and analyze the CO_2RR products, controlled potential electrolysis experiments were conducted under a CO_2 atmosphere in the −0.57 to −0.77 V potential range. The chronoamperograms (Figure 3B) indicated current densities ranging from 0.5 to 1.9 mA cm^{-2} with a small increase of these values at the more applied cathodic potentials during longer CO_2RR terms, probably due to local pH changes occurring at the electrode surface. After each experiment, the solution was examined by nuclear magnetic resonance (NMR), and we found no evidence for the presence of the porphyrin ligand fragments, thus eliminating long-term degradation of the metalloporphyrin in these conditions.[12] In addition, further reduction of Co(I)TMPyP which is involved in CO_2RR electrocatalysis[68,69] to a Co(0) porphyrin with consequent possible demetallation is unlikely since the Co(I) porphyrin π anion radical would have been formed.[68,69]

https://doi.org/10.1021/acsaem.1c01978
ACS Appl. Energy Mater. 2021, 4, 10033−10041

Scheme 2. Schematic Representation of the Suggested Mechanism of CO_2 Electroreduction to CO and CH_4 with CoPCGF Coatings on Carbon Paper Electrodes

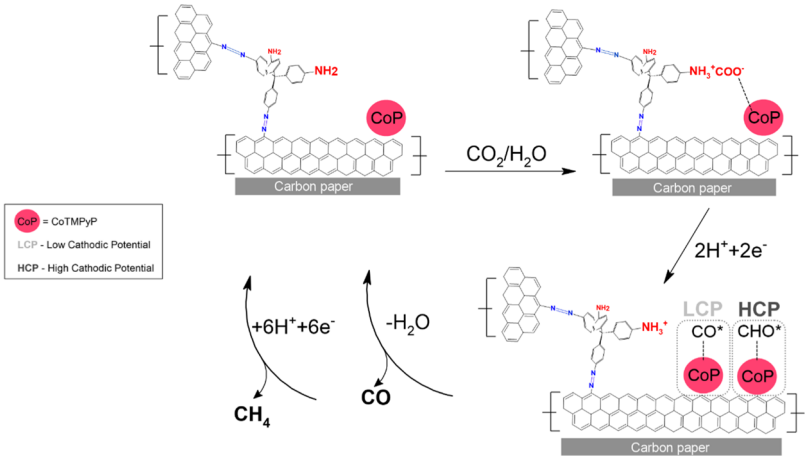

The corresponding FEs as a function of the applied potential are depicted in Figure 3C. The gaseous products of CO_2RR and hydrogen evolution reaction were analyzed by on-line gas chromatography, while no liquid products were detected by NMR. The results reveal that CO, CH_4, and H_2 are produced, and the selectivity for each product strongly depends on the applied potential. CO is initially detected with an FE of 39% at an applied potential of −0.57 V corresponding to an overpotential of 460 mV ($E^0_{CO2/CO}$ = −0.11 V vs RHE[70]). A further increase of the applied potential to −0.62 V leads to a maximum FE(CO) of 60%, while the FE(H_2) only slightly increases from 16 to 20%. CH_4 is detected with an FE of 4% at −0.67 V which corresponds to an overpotential of 840 mV for this product.[70] In addition, at this applied potential, CO generation starts to decrease (FE = 57%). By increasing the applied potential to −0.72 V, FE(CH_4) is maximized to 21% and FE(CO) dramatically decreases to 40%, clearly indicating that CO is further reduced to CH_4. HER which is suppressed at this stage gains dominance under more negative potentials [FE(H_2) of 60% at −0.77 V] and is accompanied by a large decrease of the other products (FE of 7 and 26% for CH_4 and CO, respectively). Furthermore, an experiment in the absence of CO_2 (Ar-saturated solution) for a CGF−CoTMPyP-coated electrode at −0.72 V showed low CO formation (FE = ∼ 5%, decreasing over time), no observed methane, and FE = ∼ 95% for H_2. The origin of the produced CO is likely from both remaining dissolved CO_2 in solution and adsorbed CO_2 on the coating. Similar results were obtained with electrodes coated with CGF devoid of CoTMPyP in the presence of CO_2 which revealed that HER prevails along with only a minor contribution of CO as a product of CO_2RR (FEs of CO and H_2: 2.6 and 97.4%, respectively, at −0.72 V). These last two types of experiments demonstrate that CH_4 cannot significantly form unless CoTMPyP is present in the coating and CO_2 is supplied as a reactant in the electrolyte.

We have previously reported on the catalytic behavior toward CO_2RR of dissolved CoTMPyP in neutral aqueous solutions which produces mainly H_2 and less than 10% CO.[32] Moreover, entrapment of this catalyst in electrodeposited rGO produces significant concentrations of CO and formate for CO_2RR.[33] Although CO is also formed by the same metalloporphyrin in a CGF configuration, as reported for most cobalt porphyrins,[17,23,24] substantial CH_4 formation is also observed in the present case. Shen et al. have theoretically determined that CH_4 can also be produced with such electrocatalysts by subsequent CO reduction through a concerted proton-coupled electron transfer mechanism.[71] It has also been experimentally determined that CO_2RR by a cobalt porphyrin immobilized on pyrolytic graphite leads to CH_4 but with an FE of only 0.5% at ambient conditions and an applied potential of −1.2 V versus RHE, increasing to 2.3% by increasing the CO_2 pressure to 10 atm.[25] The relatively high FE of CH_4 (∼20%) obtained at ambient conditions and a mild applied potential (∼−0.7 V vs RHE) in the present work seems to be related to the unique interactions existing when combining CoTMPyP with CGF. The presence of CGF nitrogen-CO_2 and particularly carbamate surface species, as determined to exist in this system, seems to play an important role in dictating the product profile of CO_2RR and the fate of the key intermediate species, which have been suggested to be COOH*, CO*, and CHO*.[60,72−74] The amino groups are prone to generate $-NH_3^+$ groups in aqueous solutions,[58,60] and the affinity of such a Lewis acid to the CO_2 Lewis base is able to increase the CO_2 local surface concentration. Furthermore, NH_3^+ groups have been suggested to promote adsorption of CO* and CHO* during CO_2RR in a system consisting of a Cu electrode and dissolved organic additives containing amine groups in aqueous electrolyte.[60] The same considerations in the CGF−CoTMPyP system lead to the suggestion that such strong adsorption of CO* and CHO* at the electrode surface could facilitate further electron/proton transfer from the catalyst to the carbon atom of these species toward further hydrogenation and CH_4 formation, as illustrated in Scheme 2. Although, as shown in Figure 3C, both FE(CO) and FE(H_2) increase when increasing the potential to more cathodic values up to ∼ −0.62 V, further reduction causes both decrease of CO production and suppression of FE(H_2) increase, as well as significant formation of CH_4. Applying high cathodic potentials for methane production is necessary to overcome the energy barrier related to the competitive HER[75] which predominates over CO_2RR at potentials cathodic of ∼ -0.72 V.

CONCLUSIONS

A three-dimensional azo-bonded CGF was developed by direct coupling of aromatic amino and nitro groups. The resulting porous structure exhibited irreversible CO_2 adsorption through

https://doi.org/10.1021/acsaem.1c01978
ACS Appl. Energy Mater. 2021, 4, 10033−10041

the formation of carbamate species bound to free amine groups. A CoTMPyP catalyst was successfully encapsulated in the CGF structure to form catalytic coatings on carbon paper electrodes for efficient CO_2RR. The unique properties of CGF enabled CoTMPyP to reduce CO_2 to CH_4, a rare product of CO_2RR using cobalt porphyrins, with high faradaic yields (~20%) at −0.72 V versus RHE. This is consistent with our previous reports concerning the different catalytic behavior of dissolved[32] and encapsulated CoTMPyP in electrodeposited rGO[33] toward CO_2RR and which correlated the product profile distribution with the metalloporphyrin surrounding environment. It is suggested that both the morphological and chemical structures of the new CGF/porphyrin material are responsible for allowing CO_2RR beyond the expected $2e^-$ products (CO and formate). Producing more open morphologies of the CGF/catalyst systems by using linkers with different chemical and geometrical structures [such as 1,3,5-tris(4-aminophenyl)benzene] can affect both CO_2 massive adsorption as well increasing FEs of specific products. This could inspire the development of new designed electrocatalytic structures for a variety of other reactions in the fields of fuels generation and energy conversion, such as hydrogen and oxygen reduction/evolution reactions.

■ ASSOCIATED CONTENT

Supporting Information

The Supporting Information is available free of charge at https://pubs.acs.org/doi/10.1021/acsaem.1c01978.

Materials characterization, N_2 adsorption isotherm, and photographs of the materials (PDF)

■ AUTHOR INFORMATION

Corresponding Author

Armand Bettelheim − *Chemical Engineering Department, Ben-Gurion University of the Negev, Beer-Sheva 84105, Israel*; orcid.org/0000-0003-1460-1993; Phone: 972-8-6461799; Email: armandb@bgu.ac.il

Authors

Yair Bochlin − *Chemical Engineering Department, Ben-Gurion University of the Negev, Beer-Sheva 84105, Israel*

Lior Ezuz − *Chemical Engineering Department, Ben-Gurion University of the Negev, Beer-Sheva 84105, Israel*

Yanir Kadosh − *Chemical Engineering Department, Ben-Gurion University of the Negev, Beer-Sheva 84105, Israel*

Daniel Benjamin − *Nuclear Research Center Negev, Beer Sheva 84190, Israel*

Yuval Mordekovitz − *Department of Materials Engineering, Ben-Gurion University of the Negev, Beer-Sheva 84105, Israel*

Shmuel Hayun − *Department of Materials Engineering, Ben-Gurion University of the Negev, Beer-Sheva 84105, Israel*; orcid.org/0000-0003-2179-5984

Eli Korin − *Chemical Engineering Department, Ben-Gurion University of the Negev, Beer-Sheva 84105, Israel*

Complete contact information is available at: https://pubs.acs.org/10.1021/acsaem.1c01978

Notes

The authors declare no competing financial interest.

■ REFERENCES

(1) Abanades, J. C.; Rubin, E. S.; Mazzotti, M.; Herzog, H. J. On the Climate Change Mitigation Potential of CO2 Conversion to Fuels. *Energy Environ. Sci.* **2017**, *10*, 2491−2499.

(2) Smith, P.; Davis, S. J.; Creutzig, F.; Fuss, S.; Minx, J.; Gabrielle, B.; Kato, E.; Jackson, R. B.; Cowie, A.; Kriegler, E.; Van Vuuren, D. P.; Rogelj, J.; Ciais, P.; Milne, J.; Canadell, J. G.; McCollum, D.; Peters, G.; Andrew, R.; Krey, V.; Shrestha, G.; Friedlingstein, P.; Gasser, T.; Grübler, A.; Heidug, W. K.; Jonas, M.; Jones, C. D.; Kraxner, F.; Littleton, E.; Lowe, J.; Moreira, J. R.; Nakicenovic, N.; Obersteiner, M.; Patwardhan, A.; Rogner, M.; Rubin, E.; Sharifi, A.; Torvanger, A.; Yamagata, Y.; Edmonds, J.; Yongsung, C. Biophysical and Economic Limits to Negative CO2 Emissions. *Nat. Clim. Change* **2016**, *6*, 42−50.

(3) Majumdar, A.; Deutch, J. Research Opportunities for CO2 Utilization and Negative Emissions at the Gigatonne Scale. *Joule* **2018**, *2*, 805−809.

(4) Aresta, M.; Dibenedetto, A.; Angelini, A. Catalysis for the Valorization of Exhaust Carbon: From CO2 to Chemicals, Materials, and Fuels. Technological Use of CO2. *Chem. Rev.* **2014**, *114*, 1709−1742.

(5) Chu, S.; Majumdar, A. Opportunities and Challenges for a Sustainable Energy Future. *Nature* **2012**, *488*, 294−303.

(6) Varghese, A. M.; Karanikolos, G. N. CO2 capture adsorbents functionalized by amine - bearing polymers: A review. *Int. J. Greenhouse Gas Control* **2020**, *96*, 103005.

(7) Samanta, A.; Zhao, A.; Shimizu, G. K. H.; Sarkar, P.; Gupta, R. Post-Combustion CO2 Capture Using Solid Sorbents: A Review. *Ind. Eng. Chem. Res.* **2012**, *51*, 1438−1463.

(8) Jouny, M.; Luc, W.; Jiao, F. General Techno-Economic Analysis of CO2 Electrolysis Systems. *Ind. Eng. Chem. Res.* **2018**, *57*, 2165−2177.

(9) Qiao, J.; Liu, Y.; Hong, F.; Zhang, J. A Review of Catalysts for the Electroreduction of Carbon Dioxide to Produce Low-Carbon Fuels. *Chem. Soc. Rev.* **2014**, *43*, 631.

(10) Kibria, M. G.; Edwards, J. P.; Gabardo, C. M.; Dinh, C. T.; Seifitokaldani, A.; Sinton, D.; Sargent, E. H. Electrochemical CO2 Reduction into Chemical Feedstocks: From Mechanistic Electrocatalysis Models to System Design. *Adv. Mater.* **2019**, *31*, 1807166.

(11) Finn, C.; Schnittger, S.; Yellowlees, L. J.; Love, J. B. Molecular Approaches to the Electrochemical Reduction of Carbon Dioxide. *Chem. Commun.* **2012**, *48*, 1392−1399.

(12) Marianov, A. N.; Kochubei, A. S.; Roman, T.; Conquest, O. J.; Stampfl, C.; Jiang, Y. Resolving Deactivation Pathways of Co Porphyrin-Based Electrocatalysts for CO2 Reduction in Aqueous Medium. *ACS Catal.* **2021**, *11*, 3715−3729.

(13) Göttle, A. J.; Koper, M. T. M. Determinant Role of Electrogenerated Reactive Nucleophilic Species on Selectivity during Reduction of CO2 Catalyzed by Metalloporphyrins. *J. Am. Chem. Soc.* **2018**, *140*, 4826−4834.

(14) Franco, F.; Rettenmaier, C.; Jeon, H. S.; Roldan Cuenya, B. Transition metal-based catalysts for the electrochemical CO2 reduction: from atoms and molecules to nanostructured materials. *Chem. Soc. Rev.* **2020**, *49*, 6884−6946.

(15) Sun, L.; Reddu, V.; Fisher, A. C.; Wang, X. Electrocatalytic Reduction of Carbon Dioxide: Opportunities with Heterogeneous Molecular Catalysts. *Energy Environ. Sci.* **2020**, *13*, 374−403.

(16) Choi, J.; Kim, J.; Wagner, P.; Gambhir, S.; Jalili, R.; Byun, S.; Sayyar, S.; Lee, Y. M.; MacFarlane, D. R.; Wallace, G. G.; Officer, D. L. Energy efficient electrochemical reduction of CO2 to CO using a three-dimensional porphyrin/graphene hydrogel. *Energy Environ. Sci.* **2019**, *12*, 747−755.

(17) Zhu, M.; Chen, J.; Huang, L.; Ye, R.; Xu, J.; Han, Y. F. Covalently Grafting Cobalt Porphyrin onto Carbon Nanotubes for Efficient CO 2 Electroreduction. *Angew. Chem., Int. Ed.* **2019**, *58*, 6595−6599.

(18) Jiang, L.; Fan, Z. Design of Advanced Porous Graphene Materials: From Graphene Nanomesh to 3D Architectures. *Nanoscale* **2014**, *6*, 1922−1945.

(19) Xu, C.; Xu, B.; Gu, Y.; Xiong, Z.; Sun, J.; Zhao, X. S. Graphene-Based Electrodes for Electrochemical Energy Storage. *Energy Environ. Sci.* **2013**, *6*, 1388−1414.
(20) Shen, Y.; Fang, Q.; Chen, B. Environmental Applications of Three-Dimensional Graphene-Based Macrostructures: Adsorption, Transformation, and Detection. *Environ. Sci. Technol.* **2015**, *49*, 67−84.
(21) Shen, Z.; Liu, C.; Yin, C.; Kang, S.; Liu, Y.; Ge, Z.; Xia, Q.; Wang, Y.; Li, X. Facile large-scale synthesis of macroscopic 3D porous graphene-like carbon nanosheets architecture for efficient CO2 adsorption. *Carbon* **2019**, *145*, 751−756.
(22) Tian, Y.; Lin, Y.; Hagio, T.; Hu, Y. H. Surface-Microporous Graphene for CO2 Adsorption. *Catal. Today* **2020**, *356*, 514−518.
(23) Hu, X.-M.; Rønne, M. H.; Pedersen, S. U.; Skrydstrup, T.; Daasbjerg, K. Enhanced Catalytic Activity of Cobalt Porphyrin in CO2 Electroreduction upon Immobilization on Carbon Materials. *Angew. Chem., Int. Ed.* **2017**, *56*, 6468−6472.
(24) Kumar, S.; Yadav, R. K.; Ram, K.; Aguiar, A.; Koh, J.; Sobral, A. J. F. N. Graphene Oxide Modified Cobalt Metallated Porphyrin Photocatalyst for Conversion of Formic Acid from Carbon Dioxide. *J. CO2 Util.* **2018**, *27*, 107−114.
(25) Shen, J.; Kortlever, R.; Kas, R.; Birdja, Y. Y.; Diaz-Morales, O.; Kwon, Y.; Ledezma-Yanez, I.; Schouten, K. J. P.; Mul, G.; Koper, M. T. M. Electrocatalytic Reduction of Carbon Dioxide to Carbon Monoxide and Methane at an Immobilized Cobalt Protoporphyrin. *Nat. Commun.* **2015**, *6*, 8177.
(26) Choi, J.; Wagner, P.; Jalili, R.; Kim, J.; MacFarlane, D. R.; Wallace, G. G.; Officer, D. L. A Porphyrin/Graphene Framework: A Highly Efficient and Robust Electrocatalyst for Carbon Dioxide Reduction. *Adv. Energy Mater.* **2018**, *8*, 1801280.
(27) Rao, H.; Schmidt, L. C.; Bonin, J.; Robert, M. Visible-Light-Driven Methane Formation from CO2 with a Molecular Iron Catalyst. *Nature* **2017**, *548*, 74−77.
(28) Han, Z.; Kortlever, R.; Chen, H.-Y.; Peters, J. C.; Agapie, T. CO2 Reduction Selective for C≥2 Products on Polycrystalline Copper with N-Substituted Pyridinium Additives. *ACS Cent. Sci.* **2017**, *3*, 853−859.
(29) Weng, Z.; Wu, Y.; Wang, M.; Jiang, J.; Yang, K.; Huo, S.; Wang, X. F.; Ma, Q.; Brudvig, G. W.; Batista, V. S.; Liang, Y.; Feng, Z.; Wang, H. Active Sites of Copper-Complex Catalytic Materials for Electrochemical Carbon Dioxide Reduction. *Nat. Commun.* **2018**, *9*, 415.
(30) Mohamad Latiff, N.; Fu, X.; Khairunnisa, D.; Veksha, A.; Handayani, M.; Lisak, G. Carbon Based Copper (II) Phthalocyanine Catalysts for Electrochemical CO 2 Reduction: Effect of Carbon Support on Electrocatalytic Activity. *Carbon* **2020**, *168*, 245−253.
(31) Weng, Z.; Jiang, J.; Wu, Y.; Wu, Z.; Guo, X.; Materna, K. L.; Liu, W.; Batista, V. S.; Brudvig, G. W.; Wang, H. Electrochemical CO2 Reduction to Hydrocarbons on a Heterogeneous Molecular Cu Catalyst in Aqueous Solution. *J. Am. Chem. Soc.* **2016**, *138*, 8076−8079.
(32) Bochlin, Y.; Ben-Eliyahu, Y.; Kadosh, Y.; Kozuch, S.; Zilbermann, I.; Korin, E.; Bettelheim, A. DFT and Empirical Considerations on Electrocatalytic Water/Carbon Dioxide Reduction by CoTMPyP in Neutral Aqueous Solutions**. *ChemPhysChem* **2020**, *21*, 2644−2650.
(33) Bochlin, Y.; Korin, E.; Bettelheim, A. Different Pathways for CO2 Electrocatalytic Reduction by Confined CoTMPyP in Electro-deposited Reduced Graphene Oxide. *ACS Appl. Energy Mater.* **2019**, *2*, 8434−8440.
(34) Liu, H.; Chu, J.; Yin, Z.; Cai, X.; Zhuang, L.; Deng, H. Covalent Organic Frameworks Linked by Amine Bonding for Concerted Electrochemical Reduction of CO2. *Chem* **2018**, *4*, 1696−1709.
(35) Wang, J.; Zhuang, S. Covalent Organic Frameworks (COFs) for Environmental Applications. *Coord. Chem. Rev.* **2019**, *400*, 213046.
(36) Jiang, X.; Liu, Y.; Liu, J.; Luo, Y.; Lyu, Y. Facile Synthesis of Porous Organic Polymers Bifunctionalized with Azo and Porphyrin Groups. *RSC Adv.* **2015**, *5*, 98508−98513.
(37) Chandra, S.; Kundu, T.; Kandambeth, S.; Babarao, R.; Marathe, Y.; Kunjir, S. M.; Banerjee, R. Phosphoric Acid Loaded Azo (-N=N-) Based Covalent Organic Framework for Proton Conduction. *J. Am. Chem. Soc.* **2014**, *136*, 6570−6573.
(38) Huang, N.; Wang, P.; Jiang, D. Covalent Organic Frameworks: A Materials Platform for Structural and Functional Designs. *Nat. Rev. Mater.* **2016**, *1*, 16068.
(39) Zhang, J.; Wang, L.; Li, N.; Liu, J.; Zhang, W.; Zhang, Z.; Zhou, N.; Zhu, X. A Novel Azobenzene Covalent Organic Framework. *CrystEngComm* **2014**, *16*, 6547−6551.
(40) Zhang, W.; Luo, Q.; Duan, X.; Zhou, Y.; Pei, C. Nitrated Graphene Oxide and Its Catalytic Activity in Thermal Decomposition of Ammonium Perchlorate. *Mater. Res. Bull.* **2014**, *50*, 73−78.
(41) Zhang, H.; Hines, D.; Akins, D. L. Synthesis of a Nanocomposite Composed of Reduced Graphene Oxide and Gold Nanoparticles. *Dalton Trans.* **2014**, *43*, 2670−2675.
(42) Small, L. J.; Wheeler, D. R.; Spoerke, E. D. Nanoporous Membranes with Electrochemically Switchable, Chemically Stabilized Ionic Selectivity. *Nanoscale* **2015**, *7*, 16909−16920.
(43) Peng, H.; Mo, Z.; Liao, S.; Liang, H.; Yang, L.; Luo, F.; Song, H.; Zhong, Y.; Zhang, B. High Performance Fe- and N- Doped Carbon Catalyst with Graphene Structure for Oxygen Reduction. *Sci. Rep.* **2013**, *3*, 1765.
(44) Kim, M.; Hwang, S.; Yu, J. Novel Ordered Nanoporous Graphitic C3N4 as a Support for Pt − Ru Anode Catalyst in Direct Methanol Fuel Cell. *J. Mater. Chem.* **2007**, *17*, 1656−1659.
(45) Satheesh, D.; Shanmugam, S.; Ravichandran, K. Synthesis and Characterization of Nitro-Functionalized Electrochemically Exfoliated Graphene. *Mater. Lett.* **2014**, *137*, 153−155.
(46) Pang, W.; Xue, J.; Pang, H. A High Energy Density Azobenzene/Graphene Oxide Hybrid with Weak Nonbonding Interactions for Solar Thermal Storage. *Sci. Rep.* **2019**, *9*, 5224.
(47) Zhang, W.; Ma, J.; Gao, D.; Zhou, Y.; Li, C.; Zha, J.; Zhang, J. Preparation of Amino-Functionalized Graphene Oxide by Hoffman Rearrangement and Its Performances on Polyacrylate Coating Latex. *Prog. Org. Coat.* **2016**, *94*, 9−17.
(48) Carretero, N. M.; Sandoval, S.; Casan, N.; Fuertes, A.; Tobias, G. Nitro-Graphene Oxide in Iridium Oxide Hybrids: Electrochemical Modulation of N-Graphene Redox States and Charge Capacities. *Mater. Chem. Front.* **2020**, *4*, 1421−1433.
(49) Ederer, J.; Janoš, P.; Ecorchard, P.; Tolasz, J.; Štengl, V.; Beneš, H.; Perchacz, M.; Pop-Georgievski, O. Determination of Amino Groups on Functionalized Graphene Oxide for Polyurethane Nanomaterials: XPS Quantitation vs. Functional Speciation. *RSC Adv.* **2017**, *7*, 12464−12473.
(50) Xu, Y.; Li, Z.; Zhang, F.; Zhuang, X.; Zeng, Z.; Wei, J. New nitrogen-rich azo-bridged porphyrin-conjugated microporous net-works for high performance of gas capture and storage. *RSC Adv.* **2016**, *6*, 30048−30055.
(51) Mendes, P.; Belloni, M.; Ashworth, M.; Hardy, C.; Nikitin, K.; Fitzmaurice, D.; Critchley, K.; Evans, S.; Preece, J. A Novel Example of X-Ray-Radiation-Induced Chemical Reduction of an Aromatic Nitro-Group-Containing Thin Film on SiO2 to an Aromatic Amine Film. *ChemPhysChem* **2003**, *4*, 884−889.
(52) Stankovich, S.; Dikin, D. A.; Piner, R. D.; Kohlhaas, K. A.; Kleinhammes, A.; Jia, Y.; Wu, Y.; Nguyen, S. T.; Ruoff, R. S. Synthesis of Graphene-Based Nanosheets via Chemical Reduction of Exfoliated Graphite Oxide. *Carbon* **2007**, *45*, 1558−1565.
(53) Chen, L.; Tang, Y.; Wang, K.; Liu, C.; Luo, S. Direct Electrodeposition of Reduced Graphene Oxide on Glassy Carbon Electrode and Its Electrochemical Application. *Electrochem. Commun.* **2011**, *13*, 133−137.
(54) Kaplan, A.; Korin, E.; Bettelheim, A. Structures Self-Assembled from Anionic Graphene and Cationic Manganese Porphyrin: Characterization and Application in Artificial Photosynthesis. *Eur. J. Inorg. Chem.* **2014**, *2014*, 2288−2295.
(55) Liu, S. Cooperative Adsorption on Solid Surfaces. *J. Colloid Interface Sci.* **2015**, *450*, 224−238.

https://doi.org/10.1021/acsaem.1c01978
ACS Appl. Energy Mater. 2021, 4, 10033−10041

(56) Yu, L.; Kanezashi, M.; Nagasawa, H.; Tsuru, T. Fabrication and CO2 permeation properties of amine-silica membranes using a variety of amine types. *J. Membr. Sci.* **2017**, *541*, 447−456.
(57) Yu, L.; Kanezashi, M.; Nagasawa, H.; Oshita, J.; Naka, A.; Tsuru, T. Pyrimidine-Bridged Organoalkoxysilane Membrane for High-Efficiency CO 2 Transport via Mild Affinity. *Sep. Purif. Technol.* **2017**, *178*, 232−241.
(58) Bhattacharya, M.; Sebghati, S.; Vercella, Y. M.; Saouma, C. T. Electrochemical Reduction of Carbamates and Carbamic Acids: Implications for Combined Carbon Capture and Electrochemical CO2 Recycling. *J. Electrochem. Soc.* **2020**, *167*, 086507.
(59) Yu, J.; Zhu, H.; Hao, J.; Li, H.; Li, H.; Lu, S.; Du, M. When Amine-Based Conducting Polymers Meet Au Nanoparticles: Suppressing H 2 Evolution and Promoting the Selective Electro-reduction of CO 2 to CO at Low Overpotentials. *Sustainable Energy Fuels* **2021**, *5*, 779.
(60) Qiu, Y.; Zhong, H.; Xu, W.; Zhang, T.; Li, X.; Zhang, H. Tuning the Electrocatalytic Properties of a Cu Electrode with Organic Additives Containing Amine Group for CO2 Reduction. *J. Mater. Chem. A* **2019**, *7*, 5433−5462.
(61) Lu, J.; Zhang, J. Facile Synthesis of Azo-Linked Porous Organic Frameworks via Reductive Homocoupling for Selective CO2 Capture. *J. Mater. Chem. A* **2014**, *2*, 13831−13834.
(62) D'Alessandro, D. M.; Smit, B.; Long, J. R. Carbon Dioxide Capture: Prospects for New Materials. *Angew. Chem., Int. Ed.* **2010**, *49*, 6058−6082.
(63) Zulfiqar, S.; Sarwar, M. I.; Yavuz, C. T. Melamine based porous organic amide polymers for CO2capture. *RSC Adv.* **2014**, *4*, 52263−52269.
(64) Hug, S.; Mesch, M. B.; Oh, H.; Popp, N.; Hirscher, M.; Senker, J.; Lotsch, B. V. A fluorene based covalent triazine framework with high CO2and H2capture and storage capacities. *J. Mater. Chem. A* **2014**, *2*, 5928−5936.
(65) Asai, M.; Ohba, T.; Iwanaga, T.; Kanoh, H.; Endo, M.; Campos-Delgado, J.; Terrones, M.; Nakai, K.; Kaneko, K. Marked Adsorption Irreversibility of Graphitic Nanoribbons for CO2 and H2O. *J. Am. Chem. Soc.* **2011**, *133*, 14880−14883.
(66) Ye, T.-x.; Ye, S.-l.; Chen, D.-m.; Chen, Q.-a.; Qiu, B.; Chen, X. Spectroscopic Characterization of Tetracationic Porphyrins and Their Noncovalent Functionalization with Graphene. *Spectrochim. Acta, Part A* **2012**, *86*, 467−471.
(67) Li, F.; Zhao, S.-F.; Chen, L.; Khan, A.; MacFarlane, D. R.; Zhang, J. Polyethylenimine Promoted Electrocatalytic Reduction of CO2to CO in Aqueous Medium by Graphene-Supported Amorphous Molybdenum Sulphide. *Energy Environ. Sci.* **2016**, *9*, 216−223.
(68) Ke, X.; Kumar, R.; Sankar, M.; Kadish, K. M. Electrochemistry and Spectroelectrochemistry of Cobalt Porphyrins with π-Extending and/or Highly Electron-Withdrawing Pyrrole Substituents. In Situ Electrogeneration of σ-Bonded Complexes. *Inorg. Chem.* **2018**, *57*, 1490−1503.
(69) Ke, X.; Yadav, P.; Cong, L.; Kumar, R.; Sankar, M.; Kadish, K. M. Facile and Reversible Electrogeneration of Porphyrin Trianions and Tetraanions in Nonaqueous Media. *Inorg. Chem.* **2017**, *56*, 8527−8537.
(70) Wu, J.; Huang, Y.; Ye, W.; Li, Y. CO2 Reduction: From the Electrochemical to Photochemical Approach. *Adv. Sci.* **2017**, *4*, 1700194.
(71) Shen, J.; Kolb, M. J.; Göttle, A. J.; Koper, M. T. M. DFT Study on the Mechanism of the Electrochemical Reduction of CO2 Catalyzed by Cobalt Porphyrins. *J. Phys. Chem. C* **2016**, *120*, 15714−15721.
(72) Göttle, A. J.; Koper, M. T. M. Proton-Coupled Electron Transfer in the Electrocatalysis of CO2 Reduction: Prediction of Sequential vs. Concerted Pathways Using DFT. *Chem. Sci.* **2017**, *8*, 458−465.
(73) Schouten, K. J. P.; Kwon, Y.; Van Der Ham, C. J. M.; Qin, Z.; Koper, M. T. M. A New Mechanism for the Selectivity to C1 and C2 Species in the Electrochemical Reduction of Carbon Dioxide on Copper Electrodes. *Chem. Sci.* **2011**, *2*, 1902−1909.
(74) Hirunsit, P. Electroreduction of Carbon Dioxide to Methane on Copper, Copper-Silver, and Copper-Gold Catalysts: A DFT Study. *J. Phys. Chem. C* **2013**, *117*, 8262−8268.
(75) Zhang, Y.-J.; Sethuraman, V.; Michalsky, R.; Peterson, A. A. Competition between CO2 Reduction and H2 Evolution on Transition-Metal Electrocatalysts. *ACS Catal.* **2014**, *4*, 3742−3748.

https://doi.org/10.1021/acsaem.1c01978
ACS Appl. Energy Mater. 2021, 4, 10033−10041